LETTER

https://doi.org/10.1038/s41586-019-0892-1

Two-dimensional MoS_2-enabled flexible rectenna for Wi-Fi-band wireless energy harvesting

Xu Zhang[1], Jesús Grajal[2], Jose Luis Vazquez-Roy[3], Ujwal Radhakrishna[1], Xiaoxue Wang[4], Winston Chern[1], Lin Zhou[1], Yuxuan Lin[1], Pin-Chun Shen[1], Xiang Ji[1], Xi Ling[5], Ahmad Zubair[1], Yuhao Zhang[1], Han Wang[6], Madan Dubey[7], Jing Kong[1], Mildred Dresselhaus[1,8] & Tomás Palacios[1]*

The mechanical and electronic properties of two-dimensional materials make them promising for use in flexible electronics[1–3]. Their atomic thickness and large-scale synthesis capability could enable the development of 'smart skin'[1,3–5], which could transform ordinary objects into an intelligent distributed sensor network[6]. However, although many important components of such a distributed electronic system have already been demonstrated (for example, transistors, sensors and memory devices based on two-dimensional materials[1,2,4,7]), an efficient, flexible and always-on energy-harvesting solution, which is indispensable for self-powered systems, is still missing. Electromagnetic radiation from Wi-Fi systems operating at 2.4 and 5.9 gigahertz[8] is becoming increasingly ubiquitous and would be ideal to harvest for powering future distributed electronics. However, the high frequencies used for Wi-Fi communications have remained elusive to radiofrequency harvesters (that is, rectennas) made of flexible semiconductors owing to their limited transport properties[9–12]. Here we demonstrate an atomically thin and flexible rectenna based on a MoS_2 semiconducting–metallic-phase heterojunction with a cutoff frequency of 10 gigahertz, which represents an improvement in speed of roughly one order of magnitude compared with current state-of-the-art flexible rectifiers[9–12]. This flexible MoS_2-based rectifier operates up to the X-band[8] (8 to 12 gigahertz) and covers most of the unlicensed industrial, scientific and medical radio band, including the Wi-Fi channels. By integrating the ultrafast MoS_2 rectifier with a flexible Wi-Fi-band antenna, we fabricate a fully flexible and integrated rectenna that achieves wireless energy harvesting of electromagnetic radiation in the Wi-Fi band with zero external bias (battery-free). Moreover, our MoS_2 rectifier acts as a flexible mixer, realizing frequency conversion beyond 10 gigahertz. This work provides a universal energy-harvesting building block that can be integrated with various flexible electronic systems.

Wireless power transmission dates back to Nikola Tesla's early work at the beginning of the twentieth century[13]. Efficient radiofrequency (RF) energy harvesters have been well established on rigid substrates, such as silicon[14] and III–V compounds[15,16]. However, it has been challenging to extend this technology to large-area, flexible electronic systems (such as systems that could be used in the future to monitor large infrastructures) or to enable truly ubiquitous sensing, although various flexible semiconductors have been investigated for this application. Organic semiconductors, such as pentacene, usually exhibit very low mobility (0.001–1 $cm^2\ V^{-1}s^{-1}$), which severely limits their performance in the gigahertz frequency range[17]. Metal oxides, such as amorphous indium gallium zinc oxide (IGZO), provide another option for flexible semiconductors. However, the cutoff frequency f_c of IGZO Schottky diodes, as demonstrated on flexible plastic substrates, is limited to about 1 GHz (f_c defined as the −3 dB point; see Methods)[9,10,12]. Silicon microparticles have also been fabricated into flexible diodes that exhibit a cutoff frequency of 1.6 GHz[11]. However, the random distribution of particle sizes and separation distances results in a low on/off current ratio and unreliable turn-on voltage, which deteriorates their rectification performance and reliability for large-scale production. In addition, almost all the above methods use a vertical structure to increase the effective device area and thereby to reach a sufficiently high on-current, I_{on}. However, in such a structure, the top and bottom electrodes of the diode inevitably form a parallel-plate capacitor with large parasitic capacitance, which considerably hinders its high-speed applications. Lateral p–intrinsic–n (PIN) diodes made from single-crystal silicon[18] and germanium[19] nanomembranes can be fabricated on flexible substrates for operation at 10 GHz. However, the use of PIN diodes is usually limited to RF switches and power attenuators, and such diodes are not applicable to energy harvesting[8]. Besides, the high cost of single-crystal silicon and germanium nanomembranes, as well as the complexity of their materials and processing, render them unfavourable for practical applications.

Nowadays, Wi-Fi is becoming increasingly ubiquitous in both indoor and outdoor environments and provides an abundant source of always-on RF energy. It would be highly desirable if wearable electronics could directly harvest the radiation in the Wi-Fi band (2.4 GHz and 5.9 GHz) for wireless charging. However, owing to the aforementioned challenges, a flexible RF rectifier that is fast enough to achieve Wi-Fi-band wireless energy harvesting has not been demonstrated. In this work, we present an atomically thin and fully flexible MoS_2-based rectifier with a cutoff frequency of 10 GHz at zero external bias, using a self-aligned fabrication technique. MoS_2 is an emerging two-dimensional (2D) semiconductor with high mechanical robustness and low-cost large-scale synthesis technology[2,20,21]. By patterning MoS_2 into a metallic–semiconducting (1T/1T′–2H) phase heterostructure[22] (Fig. 1a), we demonstrate a lateral Schottky diode with junction capacitance lower than 10 fF. In combination with a reduction in series resistance through self-aligned phase engineering, our MoS_2-based Schottky diode exhibits a cutoff frequency of 10 GHz (without de-embedding). This device is, to our knowledge, the first flexible rectifier with a cutoff frequency in the X-band, and it fully covers the global-satellite-positioning band (1.58 GHz and 1.22 GHz), the cellular-communications fourth-generation (4G) long-term-evolution band (1.7 GHz and 1.9 GHz), Bluetooth (2.4 GHz), the Wi-Fi channels (2.4 GHz and 5.9 GHz)[8] and even the next-generation (5G) radio system. Moreover, with an intrinsic current responsivity of up to 4.7 $A\ W^{-1}$, the performance of our 2D MoS_2 rectifier is comparable to that of rigid silicon-based Schottky diodes[23]. By integrating this ultrafast flexible MoS_2-based rectifier with a flexible Wi-Fi-band antenna, we demonstrate a fully flexible and integrated Wi-Fi-band (5.9 GHz) rectenna that can directly harvest Wi-Fi-band radiation with zero external bias (battery-free). This work can enable ubiquitous wireless charging for wearable and implantable medical sensors.

[1]Department of Electrical Engineering and Computer Science, Massachusetts Institute of Technology, Cambridge, MA, USA. [2]Information Processing and Telecommunications Center, Universidad Politécnica de Madrid, Madrid, Spain. [3]Department of Signal Theory and Communications, University Carlos III of Madrid, Madrid, Spain. [4]Department of Chemical Engineering, Massachusetts Institute of Technology, Cambridge, MA, USA. [5]Department of Chemistry, Boston University, Boston, MA, USA. [6]Ming Hsieh Department of Electrical Engineering, University of Southern California, Los Angeles, CA, USA. [7]Army Research Laboratory, Adelphi, MD, USA. [8]Department of Physics, Massachusetts Institute of Technology, Cambridge, MA, USA. *e-mail: tpalacios@mit.edu

© 2019 Springer Nature Limited. All rights reserved.

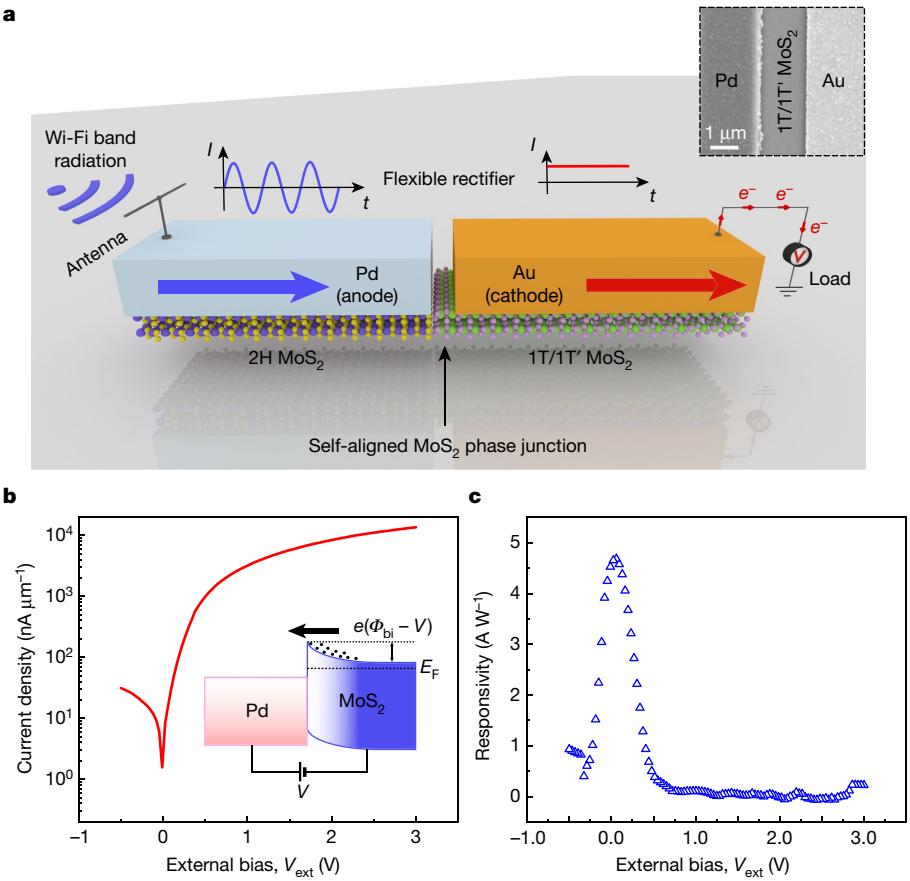

Fig. 1 | Flexible rectenna based on a 2D self-aligned MoS_2-heterostructure Schottky diode. a, Schematic of a lateral Schottky diode based on a MoS_2 semiconducting–metallic (2H–1T/1T′) phase junction. The gold layer forms an Ohmic contact with metallic (1T/1T′) MoS_2, which also forms an Ohmic contact with semiconducting (2H) MoS_2. The palladium layer forms a Schottky contact with semiconducting (2H) MoS_2. The antenna converts electromagnetic radiation in the Wi-Fi band into an a.c. signal. The lateral MoS_2 diode is fast enough to rectify the a.c. signal and generate a d.c. signal to power a load at its output. The blue and red arrows indicate a.c. and d.c. currents, respectively. Inset, scanning electron microscopy image of a MoS_2 Schottky rectifier. Channel width, 40 μm. **b**, The d.c. *I*–*V* characteristics of the MoS_2 Schottky diode in the logarithmic scale. Inset, band diagram of the MoS_2 Schottky junction under forward bias V. Φ_{bi} is the built-in potential of the MoS_2 Schottky diode, *e* is the electron charge and E_F indicates the Fermi level of the semiconducting MoS_2. **c**, Current responsivity of the MoS_2 Schottky diode at different external bias points.

We also demonstrate that our laterally designed MoS_2 diode can function as an RF mixer and successfully realize frequency conversion beyond 10 GHz. This is, to our knowledge, the best-performance MoS_2 mixer ever demonstrated on a flexible platform. This work provides building blocks that are essential for both wireless energy harvesting and wireless communication using flexible substrates.

A rectenna is a passive electronic device that directly converts an incident electromagnetic wave into direct current (d.c.) and can provide power to a load connected to its output[23]. A particularly important figure of merit of high-frequency Schottky diodes is their cutoff frequency, f_c, above which rectification is inefficient[8]. To first order, f_c is determined by the RC (resistor–capacitor) time constant of the diode[23]. To reduce the large parasitic capacitance in conventional vertical structures, we propose an MoS_2 semiconducting–metallic (2H–1T/1T′) phase junction that enables the creation of a lateral Schottky diode with ultralow RC time constant. The configuration and a scanning electron microscope image of the device are shown in Fig. 1a. The high-work-function metal palladium (Pd) was selected to form a Schottky junction with the 2H semiconducting phase MoS_2. The exposed region of MoS_2 was chemically engineered into the metallic (1T/1T′) phase whereas the Pd metal contact served as a self-aligned mask to protect the semiconducting-phase region and to define a self-aligned MoS_2 semiconducting–metallic (2H–1T/1T′) phase junction (Fig. 1a; Methods). Subsequently, gold was deposited to form an Ohmic contact[24] with 1T/1T′ MoS_2. The phase engineering of MoS_2 was investigated and confirmed by Raman spectroscopy, X-ray photoelectron spectroscopy and transport studies (Extended Data Fig. 1). The contact between 1T/1T′ MoS_2 and 2H MoS_2 was confirmed to be Ohmic and its contact resistance was obtained by the transfer-length method (Extended Data Fig. 2). Therefore, the Schottky junction between Pd and 2H MoS_2 is the dominant source of nonlinearity for rectification. The self-aligned metallic-phase region of MoS_2 is the key to reducing the series resistance of the MoS_2 Schottky diode. Meanwhile, such a lateral configuration, together with the atomic thickness of the channel region, substantially minimizes the device capacitance. We note that carbon-nanotube Schottky diodes have also been theoretically proposed as a lateral device structure for high-frequency rectification[25].

Figure 1b shows the quasi-static current–voltage (*I*–*V*) characteristics of the MoS_2 Schottky diode. The band alignment of the MoS_2 Schottky junction is shown in Fig. 1b (inset). The nonlinearity of the *I*–*V* characteristics of the MoS_2 diode has a key role in rectification. The current responsivity of a nonlinear rectifier provides a measure of the rectified d.c. output current for a given input RF power[8]. It can be calculated as (Methods)

$$R_i = \frac{\left.\frac{d^2I}{dV^2}\right|_{V=V_0}}{2\left.\frac{dI}{dV}\right|_{V=V_0}} \quad (1)$$

where V_0 is the operating bias point. As shown in Fig. 1c, the current responsivity of the MoS_2 Schottky diode around zero bias is about 4.7 A W^{-1}, which is comparable to that of rigid silicon devices[23].

To study the high-frequency performance of our lateral MoS_2 Schottky diode, we carried out scattering-parameter (S-parameter) measurements by using a vector network analyser (Keysight N5230A). A coplanar transmission line and a ground–signal–ground (G–S–G) probe configuration (Fig. 2a, top) were used to characterize the device at high frequencies[8]. We built an equivalent circuit to model the MoS_2 diode (Fig. 2a, bottom; Methods). Figure 2b, c compares the modelled and measured data of the magnitude and phase of parameter S_{11}. It can be found that the modelling result based on the equivalent circuit of Fig. 2a matches the experimental S-parameter result well. The modelled and experimental results for S_{21} and S_{22} are summarized in Extended Data Fig. 3. The S-parameter measurement allows us to obtain the resistive and capacitive components of the phase-engineered MoS_2 Schottky

© 2019 Springer Nature Limited. All rights reserved.

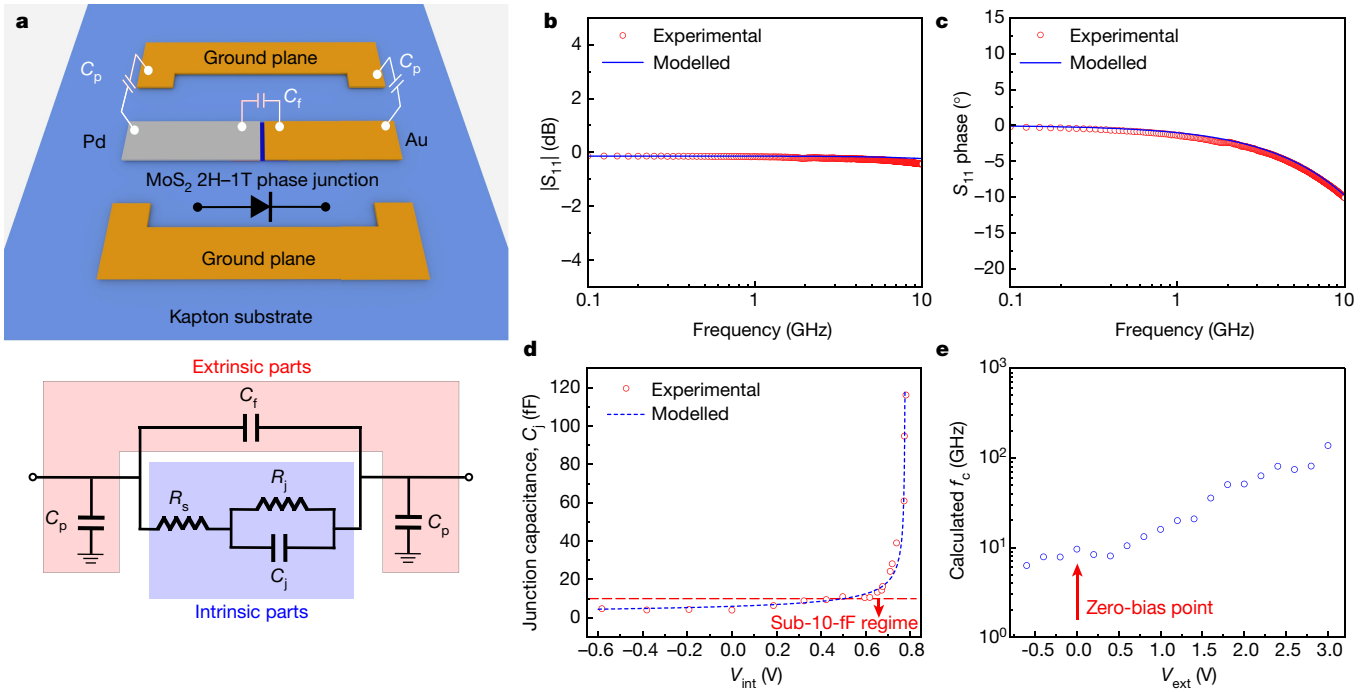

Fig. 2 | S-parameter measurements and equivalent-circuit modelling of the flexible MoS_2 rectifier. a, Top, the G–S–G coplanar configuration used for S-parameter measurements. Schematic of the origin of the fringing capacitance C_f (the capacitance between the anode and cathode metal pads) and the parasitic capacitance C_p (the capacitance between the electrodes of the diode and the ground plane). Bottom, equivalent circuit of the MoS_2 Schottky rectifier. **b**, **c**, Magnitude (**b**) and phase (**c**) of S_{11}. Blue line, modelled data; red circles, experimental data. **d**, Junction capacitance C_j obtained from the S-parameter measurements. Red circles, experimental data from the S-parameter measurement; blue dashed line, modelled data from $C_j = C_0/\sqrt{1-V/\Phi_{bi}}$. **e**, Cutoff frequency f_c, calculated using R_s, R_j and C_j values measured under different biasing conditions.

diode. Figure 2d summarizes the evolution of the junction capacitance, C_j, at different internal voltages. The internal voltage, V_{int}, is the voltage across the nonlinear junction resistance R_j only, and it can be calculated as $V_{int} = V_{ext} - I R_s$, where V_{ext} is the total voltage applied across the MoS_2 diode and R_s is the series resistance. The junction capacitance of a Schottky diode can be modelled by[26]

$$C_j = \frac{C_0}{\sqrt{1-\frac{V}{\Phi_{bi}}}} \quad (2)$$

where Φ_{bi} is the built-in potential of the MoS_2 Schottky diode and C_0 is the diode capacitance at zero bias. As shown in Fig. 2d, the experimental C_j follows the above expression (2) well. In the low-bias region ($V < 0.4$ V), the junction capacitance C_j of the MoS_2 diode is in the sub-10-fF regime (device width, 40 μm), which is at least one order of magnitude lower than the capacitance of state-of-the-art flexible rectifiers[9–12]. The series resistance R_s and junction resistance R_j are also extracted and confirmed by I–V measurements (Extended Data Fig. 4a–d; Methods). The fringing capacitance, C_f, and parasitic capacitance, C_p, are determined from S-parameter measurements to be about 10 fF and 20 fF, respectively. This result is also consistent with capacitance–voltage (C–V) measurements (Extended Data Fig. 4e; Methods).

Conventionally, the cutoff frequency of a Schottky diode is defined as the frequency at which P_j/P_{RF} drops by half compared with the value at d.c. (also known as the '−3 dB point')[8,27], where P_j is the power absorbed by the nonlinear R_j of the diode and P_{RF} is the total power absorbed by the diode. A simple analysis leads to the following expression for the cutoff frequency (Methods)[27]:

$$f_c = \frac{\sqrt{1+\frac{R_j}{R_s}}}{2\pi R_j C_j} \quad (3)$$

The cutoff frequency of our MoS_2 diode at different biases is illustrated in Fig. 2e. At zero bias, a cutoff frequency of around 10 GHz is expected, which was further examined experimentally. Because we are targeting battery-free applications of the MoS_2 rectenna, we focus only on its zero-bias operation.

As a system-level demonstrator, we built a single-stage flexible MoS_2-based RF energy-harvesting circuit (details can be found in Extended Data Fig. 5a and Methods). The circuit was first tested by generating an input RF signal using a signal generator (Keysight N5183A) and connecting it directly to the input of the MoS_2 rectifier. Figure 3a shows the rectified output voltage, V_{out}, as a function of delivered RF power, P_{RF} (that is, the power absorbed by the MoS_2 diode), at different frequencies. As expected, the rectified voltage V_{out} increases as the RF power fed into the diode increases. In the Wi-Fi band (2.4 GHz and 5.9 GHz), we calculated the RF–d.c. power conversion efficiency, which is defined as the ratio between the output d.c. power ($P_{d.c.} = V_{out}^2/R_L$, where R_L is the load resistance) and the input RF power P_{RF}, that is, $\eta = P_{d.c.}/P_{RF}$ (Fig. 3b). At 2.4 GHz, the maximum power efficiency, η_{max}, can reach 40.1% at an input power of −0.7 dBm. The results are also compared with state-of-the-art rigid-diode technology (Si and GaAs Schottky diodes) at the same frequency and the same input power level (Extended Data Fig. 5b). As shown in Fig. 3c, at an input RF power of about 5 mW, an output voltage of 3.5 V can be achieved. V_{out} drops as the input RF signal frequency increases. Our flexible MoS_2 Schottky diode exhibits a cutoff frequency of 10 GHz (using the −3 dB point definition), which is high enough to cover both of the commonly used Wi-Fi channels (2.4 GHz and 5.9 GHz).

We integrated the MoS_2 rectifier with a flexible receiver antenna fabricated on the same piece of Kapton film (Fig. 3d). The optical image of the MoS_2 rectenna is shown in Fig. 3e. The antenna was designed to have a central frequency at the 5.9 GHz Wi-Fi channel (IEEE 802.11 standards). The fabrication process is described in Methods and Extended Data Fig. 6a, b, and the electromagnetic simulation and characterization of the flexible 5.9-GHz antenna can be found

© 2019 Springer Nature Limited. All rights reserved.

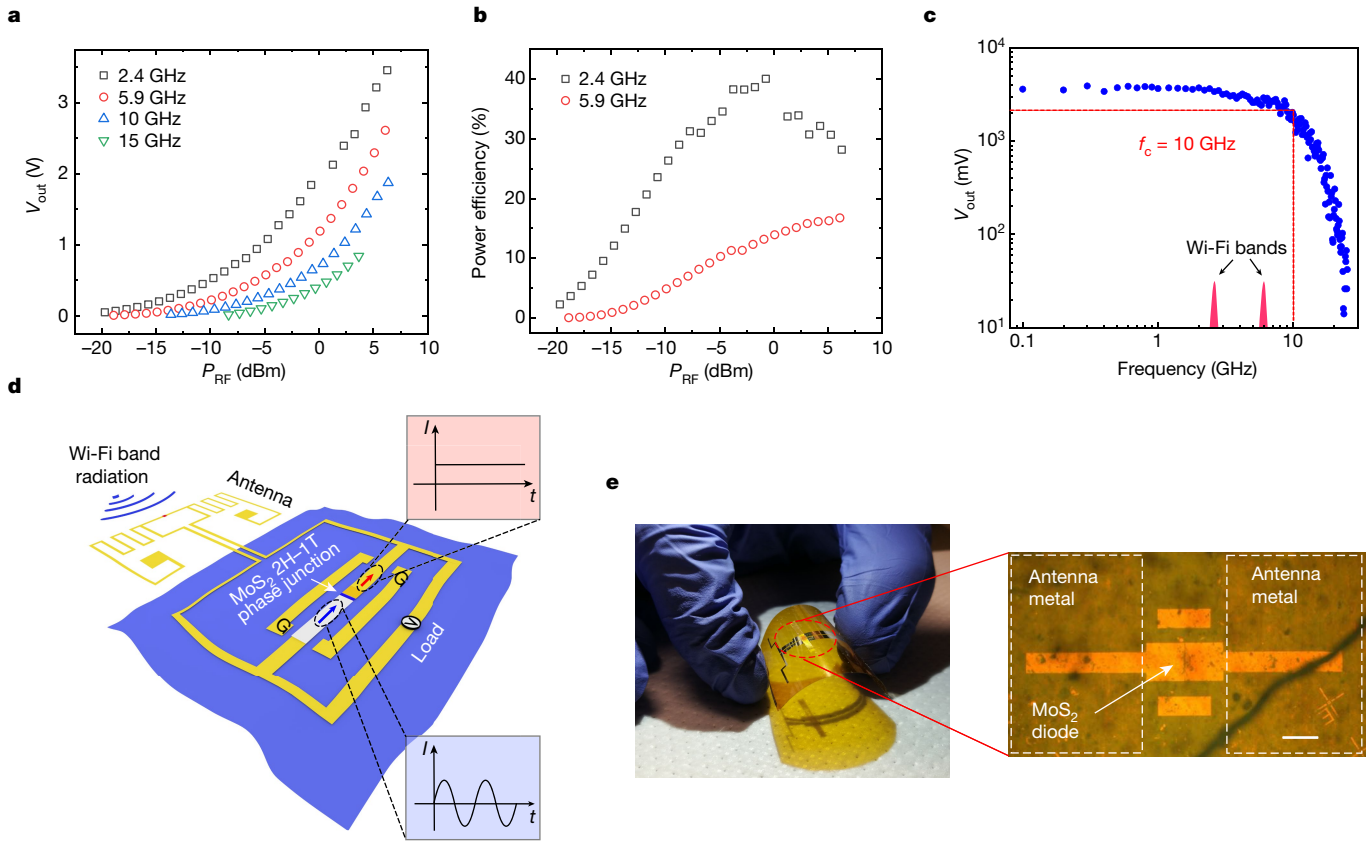

Fig. 3 | MoS_2 phase-junction rectenna as a wireless RF energy harvester. **a**, Output voltage as a function of the input RF power delivered to the device at four different frequencies (2.4 GHz, 5.9 GHz, 10 GHz and 15 GHz). The corresponding circuit diagram is shown in Extended Data Fig. 5a. **b**, Power efficiency of MoS_2 rectifiers as a function of input power in the Wi-Fi band. **c**, Output voltage as a function of frequency of the input signal for RF power $P_{RF} = 5$ mW. **d**, Illustration of a flexible rectifier based on a MoS_2 phase junction, integrated with a flexible Wi-Fi band antenna for wireless energy harvesting. The Wi-Fi-band a.c. signal from the antenna is rectified into a d.c. signal by the MoS_2 rectifier. Shown are the illustrative *I*–*t* curves corresponding to the a.c. and d.c. currents (blue and red arrow, respectively). **e**, Photograph of a MoS_2 rectenna on Kapton. The right panel shows a zoom-in of the region of the MoS_2 rectifier. Scale bar, 100 μm.

in Extended Data Fig. 6c, d. To test the entire harvesting system, we approached a commercial Wi-Fi-band transmitter antenna (powered by a signal generator with input power of about 2 mW) to the integrated MoS_2 rectenna. The flexible MoS_2 rectenna was successful in wirelessly harvesting the RF power in the Wi-Fi channel (5.9 GHz) and generated a rectified output voltage of up to 250 mV (distance from transmitter antenna, about 2.5 cm). With the demonstrated cutoff frequency (10 GHz) fully covering the Wi-Fi band, our phase-engineered MoS_2 Schottky diode enabled the experimental demonstration of a fully flexible rectenna operating as a Wi-Fi-band RF energy harvester (IEEE 802.11 standards). The complete flexibility of the MoS_2 rectenna is a critical advantage compared with rigid-diode technologies because it could enable the development of electronics with form factors that allow seamless integration with objects of arbitrary shapes.

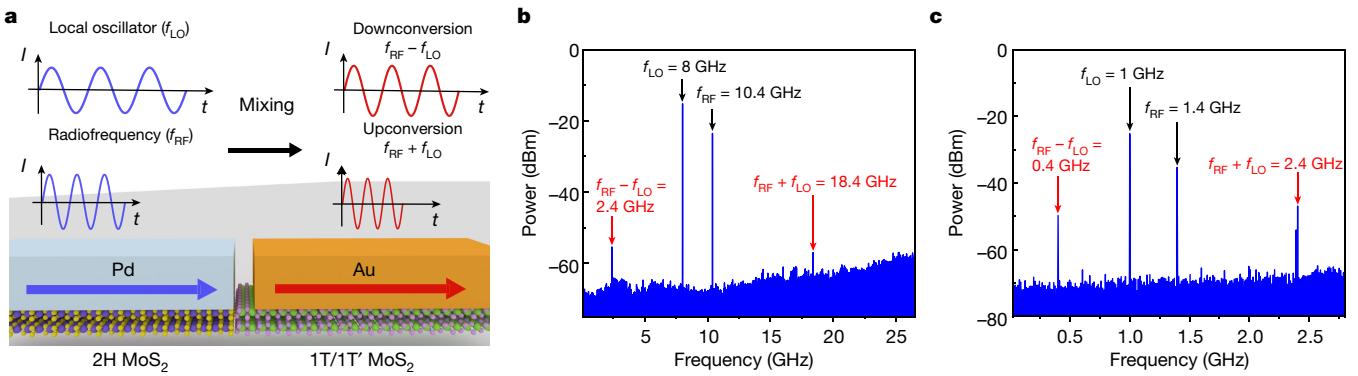

Fig. 4 | Demonstration of the MoS_2-based mixer operating in the gigahertz range. The output signals are measured by a spectrum analyser (Keysight N9020A) with an input impedance of 50 Ω. **a**, Frequency conversion by an RF mixer with two inputs: an RF signal with frequency f_{RF} and a local oscillator signal with frequency f_{LO}. A signal with frequencies $f_{IF} = f_{RF} \pm f_{LO}$ can be generated at the output of the RF mixer. **b**, Experimental demonstration of frequency conversion by a MoS_2-based gigahertz mixer. The RF and local oscillator frequencies are $f_{RF} = 10.4$ GHz and $f_{LO} = 8$ GHz, respectively. The downconverted and upconverted intermediate frequencies are $f_{IF} = 2.4$ GHz and $f_{IF} = 18.4$ GHz, respectively. **c**, Frequency conversion by a MoS_2-based gigahertz mixer. The RF and local oscillator frequencies are $f_{RF} = 1.4$ GHz and $f_{LO} = 1$ GHz, respectively. The downconverted and upconverted intermediate frequencies are $f_{IF} = 0.4$ GHz and $f_{IF} = 2.4$ GHz, respectively.

© 2019 Springer Nature Limited. All rights reserved.

The rectenna also provides a novel device architecture that could be promising for future ambient Wi-Fi energy harvesting (Methods). We note that flexible wireless energy harvesting of ambient Wi-Fi energy will require a synergistic approach incorporating innovations in circuit design, nanofabrication, device physics and system integration.

To further demonstrate the high-frequency performance of the MoS_2-based diode, we also built flexible frequency mixers on Kapton films. Frequency conversion and mixing are key building blocks of any modern wireless-communication system. A mixer based on the nonlinear I–V characteristics of the MoS_2 diode produces an output signal with frequency components at the sum and difference of its two input signals. One of the input signals is typically a local oscillator with frequency f_{LO} and the other signal is the RF carrier with frequency f_{RF}[8] (Fig. 4a). Thanks to the high-speed performance of MoS_2 Schottky diodes, we successfully demonstrated a flexible single-ended RF mixer on a Kapton substrate to realize both frequency upconversion and downconversion beyond 10 GHz. As shown in Fig. 4b, a local oscillator with $f_{LO} = 8$ GHz and an RF signal with $f_{RF} = 10.4$ GHz were combined and fed into the MoS_2 diode. At its output, both the upconverted frequency $f_{RF} + f_{LO} = 18.4$ GHz and the downconverted frequency $f_{RF} - f_{LO} = 2.4$ GHz were detected by a spectrum analyser (Keysight N9020A). When $f_{LO} = 1$ GHz and $f_{RF} = 1.4$ GHz were mixed through the MoS_2 Schottky diode, the intermediate frequencies $f_{IF} = f_{RF} + f_{LO} = 2.4$ GHz and $f_{IF} = f_{RF} - f_{LO} = 0.4$ GHz were detected (Fig. 4c). The conversion loss and 1-dB compression point are shown in Extended Data Fig. 7. We note that although a 42-GHz cutoff frequency has been reported for MoS_2 transistors on rigid substrates[28,29] for amplifier applications, to the best of our knowledge, this work is the first experimental demonstration of a flexible MoS_2-based mixer beyond 10 GHz. This MoS_2-based mixer is also advantageous over graphene-based mixers[30] in terms of system-level monolithic integration because semiconducting MoS_2 can also enable other building blocks, such as digital-logic[4] and energy-harvesting circuits.

In summary, we have described the design, fabrication and testing of an atomically thin and flexible ultrafast Schottky diode based on a MoS_2 phase heterostructure with a cutoff frequency of 10 GHz (without external bias). By integrating it with a flexible Wi-Fi-band antenna, we successfully demonstrated a fully flexible and integrated battery-free rectenna that can wirelessly harvest electromagnetic radiation in the Wi-Fi band. This work represents a key milestone for building a high-speed flexible platform that can be promising for wirelessly charging future ubiquitous electronics using the existing Wi-Fi infrastructure as an energy hotspot.

Online content

Any methods, additional references, Nature Research reporting summaries, source data, statements of data availability and associated accession codes are available at https://doi.org/10.1038/s41586-019-0892-1.

Received: 4 July 2017; Accepted: 30 November 2018;
Published online: 28 January 2019

1. Fiori, G. et al. Electronics based on two-dimensional materials. *Nat. Nanotechnol.* **9**, 768–779 (2014); erratum **9**, 1063 (2014).
2. Wang, Q. H., Kalantar-Zadeh, K., Kis, A., Coleman, J. N. & Strano, M. S. Electronics and optoelectronics of two-dimensional transition metal dichalcogenides. *Nat. Nanotechnol.* **7**, 699–712 (2012).
3. Akinwande, D., Petrone, N. & Hone, J. Two-dimensional flexible nanoelectronics. *Nat. Commun.* **5**, 5678 (2014).
4. Chhowalla, M., Jena, D. & Zhang, H. Two-dimensional semiconductors for transistors. *Nat. Rev. Mater.* **1**, 16052 (2016).
5. Mak, K. F. & Shan, J. Photonics and optoelectronics of 2D semiconductor transition metal dichalcogenides. *Nat. Photon.* **10**, 216–226 (2016).
6. Dargie, W. & Poellabauer, C. *Fundamentals of Wireless Sensor Networks: Theory and Practice* (John Wiley & Sons, Chichester, 2010).
7. Jariwala, D., Sangwan, V. K., Lauhon, L. J., Marks, T. J. & Hersam, M. C. Emerging device applications for semiconducting two-dimensional transition metal dichalcogenides. *ACS Nano* **8**, 1102–1120 (2014).
8. Pozar, D. *Microwave Engineering 4th edn* (PHI Learning Private Limited, New Delhi, 2012).
9. Chasin, A. et al. An integrated a-IGZO UHF energy harvester for passive RFID tags. *IEEE Trans. Electron Dev.* **61**, 3289–3295 (2014).
10. Chasin, A. et al. UHF IGZO Schottky diode. In *Proc. 2012 International Electron Devices Meeting* 12.4.1–12.4.4 (IEEE, 2012).
11. Sani, N. et al. All-printed diode operating at 1.6 GHz. *Proc. Natl Acad. Sci. USA* **111**, 11943–11948 (2014).
12. Zhang, J. et al. Flexible indium–gallium–zinc–oxide Schottky diode operating beyond 2.45 GHz. *Nat. Commun.* **6**, 7561 (2015).
13. Tesla, N. Apparatus for utilizing effects transmitted from a distance to a receiving device through natural media. US Patent 685, 955 (1901).
14. Strohm, K. M., Buechler, J. & Kasper, E. SIMMWIC rectennas on high-resistivity silicon and CMOS compatibility. *IEEE Trans. Microw. Theory Tech.* **46**, 669–676 (1998).
15. Suh, Y.-H. & Chang, K. A high-efficiency dual-frequency rectenna for 2.45- and 5.8-GHz wireless power transmission. *IEEE Trans. Microw. Theory Tech.* **50**, 1784–1789 (2002).
16. Sizov, F. & Rogalski, A. THz detectors. *Prog. Quantum Electron.* **34**, 278–347 (2010).
17. Steudel, S. et al. Ultra-high frequency rectification using organic diodes. In *Proc. 2008 IEEE International Electron Devices Meeting* 1–4 (IEEE, 2008).
18. Seo, J.-H. et al. Investigation of various mechanical bending strains on characteristics of flexible monocrystalline silicon nanomembrane diodes on a plastic substrate. *Microelectron. Eng.* **110**, 40–43 (2013).
19. Qin, G. et al. Fabrication and characterization of flexible microwave single-crystal germanium nanomembrane diodes on a plastic substrate. *IEEE Electron Device Lett.* **34**, 160–162 (2013).
20. Hsu, A. et al. Large-area 2-D electronics: materials, technology, and devices. *Proc. IEEE* **101**, 1638–1652 (2013).
21. Lee, Y.-H. et al. Synthesis of large-area MoS_2 atomic layers with chemical vapor deposition. *Adv. Mater.* **24**, 2320–2325 (2012).
22. Kappera, R. et al. Phase-engineered low-resistance contacts for ultrathin MoS_2 transistors. *Nat. Mater.* **13**, 1128–1134 (2014).
23. Donchev, E. et al. The rectenna device: from theory to practice (a review). *MRS Energy Sustain.* **1**, E1 (2014); corrigendum **1**, E5 (2014).
24. English, C. D., Shine, G., Dorgan, V. E., Saraswat, K. C. & Pop, E. Improved contacts to MoS_2 transistors by ultra-high vacuum metal deposition. *Nano Lett.* **16**, 3824–3830 (2016).
25. Manohara, H. M., Wong, E. W., Schlecht, E., Hunt, B. D. & Siegel, P. H. Carbon nanotube Schottky diodes using Ti–Schottky and Pt–Ohmic contacts for high frequency applications. *Nano Lett.* **5**, 1469–1474 (2005).
26. Sze, S. M. & Ng, K. K. *Physics of Semiconductor Devices*. (Wiley, 2007).
27. Cowley, A. M. & Sorensen, H. O. Quantitative comparison of solid-state microwave detectors. *IEEE Trans. Microw. Theory Tech.* **14**, 588–602 (1966).
28. Park, S. et al. High-frequency prospects of 2D nanomaterials for flexible nanoelectronics from baseband to sub-THz devices. In *Proc. 2015 IEEE International Electron Devices Meeting* 32.1.1–32.1.4 (IEEE, 2015).
29. Cheng, R. et al. Few-layer molybdenum disulfide transistors and circuits for high-speed flexible electronics. *Nat. Commun.* **5**, 5143 (2014).
30. Wang, H., Hsu, A., Wu, J., Kong, J. & Palacios, T. Graphene-based ambipolar RF mixers. *IEEE Electron Device Lett.* **31**, 906–908 (2010).

Acknowledgements This work was financially supported by the MIT/Army Institute for Soldier Nanotechnologies, the Army Research Laboratory (grant W911NF-14-2-0102), the STC Center for Integrated Quantum Materials (National Science Foundation (NSF) grant number DMR-1231319), the Air Force Office of Scientific Research under the MURI-FATE program (grant number FA9550-15-1-0514), NSF grant DMR-1507806, the NSF Center for Energy Efficient Electronics Science (E^3S; NSF grant number ECCS-0939514) and MIT International Science and Technology Initiatives (MISTI). Device fabrication was carried out at the MIT Microsystems Technology Laboratories. X-ray spectroscopy studies were done at the Cornell Center for Materials Research Shared Facilities. We acknowledge K. Gleason and A. Nourbakhsh for discussions.

Reviewer information *Nature* thanks F. Schwierz and the other anonymous reviewer(s) for their contribution to the peer review of this work.

Author contributions X.Z. and T.P. conceived and designed the experiments. X.Z. fabricated the flexible devices. J.G., X.Z. and U.R. carried out the high-frequency measurements. J.G. and X.Z. did the circuit modelling and data analysis. X.W. and X.Z. performed the chemical phase change of the MoS_2 samples. X.Z., X.W. and L.Z. conducted the spectroscopic study. W.C. and X.Z. carried out the C–V measurement. J.L.V.R. and J.G. designed and fabricated the flexible antenna. All authors contributed to interpreting the data and writing the manuscript.

Competing interests The authors declare no competing interests.

Additional information
Extended data is available for this paper at https://doi.org/10.1038/s41586-019-0892-1.
Reprints and permissions information is available at http://www.nature.com/reprints.
Correspondence and requests for materials should be addressed to T.P.
Publisher's note: Springer Nature remains neutral with regard to jurisdictional claims in published maps and institutional affiliations.

© 2019 Springer Nature Limited. All rights reserved.

METHODS

Rectenna fabrication and integration. We fabricated flexible high-speed rectifiers based on MoS_2 semiconducting–metallic (2H–1T/1T′) phase junctions. Few-layer MoS_2 was obtained by exfoliation from bulk crystals. All the fabrication was done on flexible DuPont Kapton polyimide films with a thickness of 50.8 μm. Electron-beam lithography (EBL) with PMMA (poly(methyl methacrylate)) as the electron-beam resist was used to define the Schottky contact region on semiconducting (2H) MoS_2. To avoid charging effects on the insulating Kapton substrate during EBL, we coated the PMMA with a layer of the conductive liquid Espacer (purchased from Showa Denko) as a charge-dissipating agent. After EBL, the Espacer was rinsed off with distilled water before the development of the PMMA resist. Then a 50-nm-thick layer of palladium (Pd) was deposited to form a Schottky contact with MoS_2 by electron-beam evaporation. After the formation of the Schottky contact, the Kapton film with the Pd/MoS_2 structure was immersed into 1.6 M n-butyllithium (from Sigma Aldrich) solution for 10 min to convert the exposed region of the MoS_2 into the metallic phase[22]. This process was performed in the N_2 atmosphere of a glove box. X-ray photoelectron spectroscopy and Raman spectroscopy were carried out to confirm the phase transition of MoS_2 (Extended Data Fig. 1a, b). The 1T-phase MoS_2 is metastable under ambient conditions, and part of the 1T region is converted into the 1T′ phase. However, the 1T/1T′-mixture MoS_2 remains metallic even after baking (180 °C for 3 min; see Extended Data Fig. 1c). The Pd metal contact served as a self-aligned mask to protect the 2H semiconducting region of MoS_2 lying underneath. Then the Kapton film was rinsed thoroughly with hexane to remove any lithium residue. A second EBL process was performed to define the Ohmic contact region with the phase-engineered MoS_2. Then a 50-nm-thick gold (Au) layer was deposited by electron-beam evaporation in high vacuum (10^{-8} torr) to form an Ohmic contact with MoS_2. Finally, the coplanar transmission line (G–S–G) structure (5 nm Ti/50 nm Au) was fabricated by EBL for high-frequency S-parameter measurements. The reduction of the RC time constant, which is due to self-aligned phase engineering and the lateral structure of the diode, is largely immune to the partial 1T-to-1T′ phase conversion. Our MoS_2 rectenna can operate stably under ambient conditions for at least one year without noticeable degradation.

The Wi-Fi-band receiver antenna was designed using the CST Microwave Studio software. The flexible antenna was fabricated by electron-beam evaporation of 5 nm Ti and 70 nm Au on a 50.8-μm-thick Kapton thin film. The integration process is illustrated in Extended Data Fig. 6a, b. The electromagnetic simulation and return loss measurements of the flexible antenna are shown in Extended Data Fig. 6c, d. Its central frequency is about 5.9 GHz.

After the above processes, MoS_2 phase-junction-diode arrays were first fabricated on a Kapton film. The G–S–G device configuration of the MoS_2 diode allows high-frequency S-parameter measurements. The MoS_2 diode was subsequently electrically connected with the receiver antenna. The MoS_2 diode and the receiver antenna were aligned so that the two terminals of the signal line were electrically connected to the two transmission lines of the receiver antenna. The length of the G line (170 μm) was designed to be shorter than the gap between the antenna transmission lines (250 μm) to avoid shorting effects (Fig. 3e). In addition, the length of the signal line (1 mm) was designed to be larger than the gap between the antenna transmission lines (250 μm) to allow electrical connection. During the demonstration of energy harvesting, a commercial transmitter Wi-Fi-band antenna was powered by a signal generator (Keysight N5183A) and approached the MoS_2 rectenna (Extended Data Fig. 6b). The rectified output voltage V_{out} was measured by an oscilloscope with impedance of 1 MΩ (Keysight DSO6054A). The rectenna was connected to an oscilloscope through an SMA connector. A load resistance of 10 kΩ was connected with the oscilloscope in a parallel configuration (Extended Data Fig. 5a), so the effective output resistance was about 10 kΩ. The input power available to the MoS_2 rectenna was about 3 dBm (about 2 mW). The distance between our flexible rectenna and a commercial Wi-Fi-band antenna (PCB Yagi; gain of 2 dBi (decibels relative to isotropic)), which was powered by a signal generator (continuous wave), was about 2.5 cm. The orientation of the MoS_2 rectenna was optimized with respect to the commercial Wi-Fi antenna to maximize the collection of RF power.

S-parameter measurement and equivalent-circuit modelling. To characterize the high-frequency performance of our MoS_2 Schottky diode, we performed S-parameter measurements using a vector network analyser (VNA; Keysight N5230A). The two-channel microwave receiver of the VNA allowed us to measure the magnitude and phase of the transmitted and reflected waves from the device. Two transmission-line cables with impedance of 50 Ω were connected to the device under test through G–S–G probes. A proper calibration was done to eliminate the extrinsic effects and the systematic error of the measurement system[8]. The RF source was set to sweep from 100 MHz to 20 GHz, and an internal reflectometer was used to detect the incident, reflected and transmitted RF waves. The magnitude and phase of S_{11}, S_{21}, S_{12} and S_{22} were measured and recorded (Fig. 2b, c, Extended Data Fig. 3). S_{11} represents the reflection coefficient at the input port, whereas S_{22} represents the reflection coefficient at the output port. S_{21} is a measure of the insertion loss of the device under test, and S_{12} characterizes the isolation from the output to the input. The S-parameter measurements were repeated with the device under test biased at different bias points from −0.6 V to 3 V. The S-parameters were measured when the MoS_2 Schottky diode was under non-bending conditions.

To gain further insight into the capacitive and resistive components of the MoS_2 diode, we built a small-signal equivalent circuit to model the device using Keysight's Advanced Design System. A schematic of the simulation circuit is shown in Fig. 2a. The internal part of the MoS_2 diode was modelled by the series resistance R_s, the nonlinear junction resistance R_j and the junction capacitance C_j. The series resistance R_s includes the Ohmic contact resistance of the diode. The junction resistance R_j represents the nonlinear resistance of the Schottky junction, which is bias-dependent. The junction capacitance of the diode, C_j, is also bias-dependent. The external parasitics of the MoS_2 diode were also considered and analysed: C_f denotes the fringing capacitance between the diode's anode and cathode metal pads. C_p incorporates the parasitic capacitance between the electrodes of the diode and the ground plane (Fig. 2a). A quasi-Newton algorithm was used to optimize the parameters of the model. As illustrated in Fig. 2b, c and Extended Data Fig. 3, the simulated S-parameters match well the measured S-parameters.

The series resistance R_s and the junction resistance R_j can be obtained from the experimental S-parameters (Extended Data Fig. 4a, b). Extended Data Fig. 4a shows R_s as a function of the applied bias. The series resistance R_s increases slightly from 2,400 Ω to 3,400 Ω as the applied bias increases from −0.6 V to 3 V. The semiconducting MoS_2 region incorporates two parts: a depletion region and a quasi-neutral region (that is, regions without band bending). As the bias increases, the depletion region of MoS_2 shrinks, which can be seen from the conventional depletion-thickness formula[25] in a Schottky diode $x_d = \sqrt{2\epsilon(\Phi_{bi} - V)/eN_d}$, where ϵ is the permittivity of MoS_2, Φ_{bi} is the built-in potential, V is the applied bias, e is the electron charge and N_d is the doping level of MoS_2. As the depletion region of MoS_2 shrinks, the quasi-neutral region of MoS_2 expands and contributes to an increased series resistance R_s. The junction resistance R_j decreases as the diode is turned on (Extended Data Fig. 4b). The R_s and R_j values obtained from the S-parameter measurements were also confirmed by quasi-static I–V measurement and modelling (Extended Data Fig. 4c, d). Similarly, the junction capacitance C_j can be extracted from the measured S-parameters. Figure 2d summarizes the evolution of C_j at different internal biases. We attribute the ultralow junction capacitance of the device to its lateral structure. In such a lateral device structure, the charge transport across the Schottky barrier mainly occurs near the MoS_2 phase boundary, with an extension within a transfer length, which is usually less than 1 μm[24,31]. The transfer length[26] is the distance beyond which the current density drops by 1/e. In other words, the applied bias mainly drops across the region near the MoS_2 phase boundary, and therefore the modulation of the depletion region of MoS_2 mainly occurs within one transfer length. Consequently, the effective area of the Schottky junction, and thus the junction capacitance C_j, is substantially reduced. We also expect that the novel device architecture presented in this work could inspire new designs for other types of high-frequency devices to further improve high-speed performance. From Fig. 2d, the built-in potential Φ_{bi} of the MoS_2–Pd Schottky junction can be extracted to be about 0.78 eV on the basis of equation (2). The extrinsic parasitics can also be obtained using equivalent-circuit modelling (Fig. 2a, bottom): the fringing capacitance C_f is about 10 fF, and the parasitic capacitance C_p is about 20 fF. Thanks to the lateral design of our MoS_2 rectifier, the total capacitance of the device is about $C_f + C_p + C_j \approx 40$ fF (when one terminal of the circuit in Fig. 2a is grounded). This value is about one order of magnitude smaller than that of state-of-the-art flexible rectifiers[9–12]. This is also confirmed by C–V measurements (Extended Data Fig. 4e).

RF–d.c. power conversion efficiency and Wi-Fi-band energy harvesting. For the characterization in Fig. 3a–c, the rectified output voltage V_{out} was measured using an oscilloscope with impedance of 1 MΩ, which was in shunt with a load resistance. The optimum load resistance was found to be about 10 kΩ. At 2.4 GHz, the power efficiency of our flexible MoS_2 rectifiers was in the range 10%–40% for input power between −15 dBm and 5 dBm (Fig. 3b). Our MoS_2 rectifiers exhibit competitive power efficiency; for comparison, the state-of-the-art rigid Si and GaAs Schottky diodes can reach a power efficiency of 5%–70% at the same frequency and the same range of input power (Extended Data Fig. 5b). The maximum power efficiency, η_{max}, of our MoS_2 rectifiers at 2.4 GHz was observed around an input RF power of −0.7 dBm ($\eta_{max} \approx 40.1\%$). The ambient Wi-Fi power collected by a 2.4-GHz Wi-Fi antenna is $P_{in} = W_s A_{eff} = [(P_{TX}G_{TX})/(4\pi d^2)]\,[(G_{RX}\lambda^2)/(4\pi)] = \{(1\text{ W})/[4\pi(100\text{ cm})^2]\}[1.58(12.5\text{ cm})^2/(4\pi)] \approx 156$ μW (that is, −8 dBm), where P_{in} is the input power to the receiver antenna, W_s is the ambient Wi-Fi power density, A_{eff} is the effective receiver antenna area, P_{TX} is the total power of the transmitter antenna, G_{TX} is the gain of the transmitter antenna, d is the distance to the transmitter antenna (assuming a distance of 1 m), G_{RX} is the gain of the receiver antenna (about 2 dBi in our flexible antenna design; that is, a power ratio of 1.58) and λ

© 2019 Springer Nature Limited. All rights reserved.

is the wavelength[32]. We note that $P_{TX}G_{TX}$ is the equivalent isotropically radiated power (EIRP), and we use 1 W as a typical EIRP value for a 2.4-GHz Wi-Fi transmitter antenna. The EIRP may vary in different regions in the world; for example, in the United States the EIRP (2.4 GHz) is 1 W[33]. At 2.4 GHz, the power efficiency of our MoS_2 device is about 31% (at $P_{in} = -8$ dBm; see Fig. 3b). Therefore, even in this proof-of-concept demonstration, the output d.c. power of our MoS_2-based rectifier reached about $P_{out} = P_{in} \times \eta = (156\ \mu W) \times 31\% = 48.4\ \mu W$ at the input power level of −8 dBm (at 2.4 GHz). It should be noted that in this work this level of output power was achieved in an academic laboratory and had not yet been optimized. In our current MoS_2 device (with channel width $W = 40\ \mu m$), the maximum power efficiency (about 40.1%) occurs at an input power of −0.7 dBm. On the basis of microwave theory, the maximum power efficiency η_{max} can be shifted to lower input power (for example, −8 dBm) by reducing the device area[34], which in our case is the channel width. Given the relatively large channel width ($W = 40\ \mu m$) used in our current design, it is possible to reduce the channel width and tune the η_{max} point to a lower power level. By shifting η_{max} to −8 dBm, we can potentially harvest an output d.c. power of $(156\ \mu W) \times 40.1\% = 62.6\ \mu W$ out of the ambient Wi-Fi band energy. Through optimization of the material engineering, the phase-change process and the circuit, the power efficiency of the presented MoS_2-based rectifiers can be further improved.

Theory of nonlinear diode rectification. A diode is a two-terminal electronic device with nonlinear *I*–*V* characteristics. This nonlinearity is fundamental for many useful applications, such as rectification, detection and frequency mixing[8]. The d.c. *I*–*V* characteristics of a Schottky diode can be modelled by $I(V) = I_s(e^{\alpha V} - 1)$, where $\alpha = e/(nk_BT)$, I_s is the reverse saturation current, k_B is the Boltzmann constant, T is the temperature, e is the electron charge and n is the ideality factor. In a small-signal model, the $I(V)$ relation can be expanded in a Taylor series at $V = V_0$:

$$I(V) = I_0 + \Delta V \frac{dI}{dV}\bigg|_{V=V_0} + \frac{1}{2}\Delta V^2 \frac{d^2I}{dV^2}\bigg|_{V=V_0} + \dots \tag{4}$$

where $I_0 = I(V_0)$ and $\Delta V = V - V_0$.

In a small-signal approximation, we can write the input voltage as

$$V = V_0 + A\cos(\omega t) \tag{5}$$

where A is the amplitude of the microwave input signal. By plugging (5) into (4), the diode current becomes

$$\begin{aligned} I(V) &= I_0 + A\cos(\omega t)\frac{dI}{dV}\bigg|_{V=V_0} + \frac{1}{2}A^2\cos^2(\omega t)\frac{d^2I}{dV^2}\bigg|_{V=V_0} + \dots = \\ &= I_0 + \frac{1}{4}A^2\frac{d^2I}{dV^2}\bigg|_{V=V_0} + A\cos(\omega t)\frac{dI}{dV}\bigg|_{V=V_0} + \frac{1}{2}A^2\cos(2\omega t)\frac{d^2I}{dV^2}\bigg|_{V=V_0} \\ &\quad + \dots \end{aligned} \tag{6}$$

It can be seen from the above expression that the output signal contains d.c. components and RF signals with frequencies ω and 2ω (as well as other higher-order harmonics). The rectified d.c. current $I_{d.c.}$ is the second term,

$$\frac{1}{4}A^2\frac{d^2I}{dV^2}\bigg|_{V=V_0} \tag{7}$$

The intrinsic current responsivity R_i is defined as the ratio of the rectified d.c. current $I_{d.c.}$ and the RF power delivered to the nonlinear junction resistance P_{in}. P_{in} can be obtained from the time-averaged integration of

$$\frac{1}{T}\int_0^T I(t)V(t)\,dt = \frac{1}{2}A^2\frac{dI}{dV}\bigg|_{V=V_0} \tag{8}$$

Therefore,

$$R_i = \frac{I_{d.c.}}{P_{in}} = \frac{\frac{d^2I}{dV^2}\Big|_{V=V_0}}{2\frac{dI}{dV}\Big|_{V=V_0}} \tag{9}$$

In the calculation of the intrinsic responsivity in Fig. 1c, 10-point Savitzky–Golay smoothing was used to obtain the average of the slopes.

Analysis of the cutoff frequency, f_c. In this work, the cutoff frequency of a high-speed diode is defined by the conventional −3 dB point, which is different from the cutoff frequency defined for traditional transistors (that is, the unit-gain point). Here we explain in detail how the cutoff frequency f_c of our MoS_2 Schottky diode is defined. The internal part of a Schottky diode can be modelled by a series resistance R_s, a junction resistance R_j and a junction capacitance C_j, as indicated in Fig. 2a. Let us denote the total voltage applied across the intrinsic diode as V and the voltage across R_j as V_j. The overall impedance of the diode is represented by Z. We note that not all of the incident RF power absorbed by the MoS_2 Schottky diode is consumed by the nonlinear junction resistance R_j. Part of the RF power is dissipated in the series resistance R_s. The RF power absorbed by the diode can be calculated as[27]

$$P_{RF} = \frac{|V|^2}{2}\mathrm{Re}\left(\frac{1}{Z}\right) \tag{10}$$

where

$$Z = R_s + \frac{1}{\frac{1}{R_j} + i\omega C_j} \tag{11}$$

and i is the imaginary unit. By plugging Z into (10), we can get

$$P_{RF} = \frac{|V|^2}{2}\frac{\frac{1}{R_j}\left(1 + \frac{R_s}{R_j}\right) + \omega^2 C_j^2 R_s}{\left(1 + \frac{R_s}{R_j}\right)^2 + \omega^2 C_j^2 R_s^2} \tag{12}$$

The voltage across R_j can be calculated as

$$\begin{aligned} |V_j|^2 &= |V|^2 \left| \frac{\frac{1}{\frac{1}{R_j} + i\omega C_j}}{\frac{1}{\frac{1}{R_j} + i\omega C_j} + R_s} \right|^2 \\ &= |V|^2 \left| \frac{1}{1 + \frac{R_s}{R_j} + i\omega C_j R_s} \right|^2 \\ &= \frac{|V|^2}{\left(1 + \frac{R_s}{R_j}\right)^2 + \omega^2 C_j^2 R_s^2} \end{aligned} \tag{13}$$

Therefore, P_{RF} can be expressed in terms of V_j as follows

$$P_{RF} = \frac{|V|^2}{2}\frac{\frac{1}{R_j}\left(1 + \frac{R_s}{R_j}\right) + \omega^2 C_j^2 R_s}{\left(1 + \frac{R_s}{R_j}\right)^2 + \omega^2 C_j^2 R_s^2} = \frac{|V_j|^2}{2}\left[\frac{1}{R_j}\left(1 + \frac{R_s}{R_j}\right) + \omega^2 C_j^2 R_s\right] \tag{14}$$

The part of the incident power consumed by R_j is

$$P_j = \frac{|V_j|^2}{2R_j} \tag{15}$$

so

$$\frac{P_j}{P_{RF}} = \frac{1}{1 + \frac{R_s}{R_j} + \omega^2 C_j^2 R_s R_j} = \frac{1}{\left(1 + \frac{R_s}{R_j}\right)\left(1 + \frac{\omega^2 C_j^2 R_s R_j}{1 + \frac{R_s}{R_j}}\right)} \tag{16}$$

By defining the cutoff frequency f_c as the frequency at which P_j/P_{RF} is half of its value at d.c. (that is, the −3 dB point), we have

$$\frac{P_j}{P_{RF}} = \frac{1}{\left(1 + \frac{R_s}{R_j}\right)\left[1 + \left(\frac{f}{f_c}\right)^2\right]} \tag{17}$$

By using this definition of the −3 dB point, f_c can be obtained as

$$f_c = \frac{\sqrt{1 + \frac{R_j}{R_s}}}{2\pi R_j C_j}$$

Extended Data Table 1 summarizes the cutoff frequency and solid-state properties of state-of-the-art flexible semiconductors and rigid silicon.

© 2019 Springer Nature Limited. All rights reserved.

Data availability

The data that support the findings of this study are available from the corresponding author on reasonable request.

31. Guo, Y. et al. Study on the resistance distribution at the contact between molybdenum disulfide and metals. *ACS Nano* **8**, 7771–7779 (2014).
32. Mou, J., Xue, Q., Guo, D. & Lv, X. A THz detector chip with printed circular cavity as package and enhancement of antenna gain. *IEEE Trans. Antenn. Propag.* **64**, 1242–1249 (2016).
33. van Hattem, R. Maximum wifi transmission power per country. Wolph https://w.wol.ph/2015/08/28/maximum-wifi-transmission-power-country/ (2015).
34. Grajal, J., Krozer, V., Gonzalez, E., Maldonado, F. & Gismero, J. Modeling and design aspects of millimeter-wave and submillimeter-wave Schottky diode varactor frequency multipliers. *IEEE Trans. Microw. Theory Tech.* **48**, 700–711 (2000).
35. Valenta, C. R. & Durgin, G. D. Harvesting wireless power: survey of energy-harvester conversion efficiency in far-field, wireless power transfer systems. *IEEE Microw. Mag.* **15**, 108–120 (2014).
36. Mbombolo, S. E. F. & Park, C. W. An improved detector topology for a rectenna. In *Proc. 2011 IEEE MTT-S International Microwave Workshop Series on Innovative Wireless Power Transmission: Technologies, Systems, and Applications* 23–26 (IEEE, 2011).
37. Olgun, U., Chen, C. & Volakis, J. L. Investigation of rectenna array configurations for enhanced RF power harvesting. *IEEE Antennas Wirel. Propag. Lett.* **10**, 262–265 (2011).
38. Olgun, U., Chen, C. & Volakis, J. L. Wireless power harvesting with planar rectennas for 2.45 GHz RFIDs. In *Proc. 2010 URSI International Symposium on Electromagnetic Theory* 329–331 (IEEE, 2010).
39. Wang, D. & Negra, R. Design of a rectifier for 2.45 GHz wireless power transmission. In PRIME 2012; 8th Conference on Ph.D. Research in Microelectronics & Electronics (VDE, 2012).
40. Kim, J. & Jeong, J. Design of high efficiency rectifier at 2.45 GHz using parasitic canceling circuit. *Microw. Opt. Technol. Lett.* **55**, 608–611 (2013).
41. Bertolazzi, S., Brivio, J. & Kis, A. Stretching and breaking of ultrathin MoS_2. *ACS Nano* **5**, 9703–9709 (2011).
42. Kwon, J.-Y., Lee, D.-J. & Kim, K.-B. Transparent amorphous oxide semiconductor thin film transistor. *Electron. Mater. Lett.* **7**, 1–11 (2011).
43. Mohammed, D. W. et al. Mechanical properties of amorphous indium–gallium–zinc oxide thin films on compliant substrates for flexible optoelectronic devices. *Thin Solid Films* **594**, 197–204 (2015).
44. Freund, L. B. & Suresh, S. *Thin Film Materials: Stress, Defect Formation and Surface Evolution* (Cambridge Univ. Press, Cambridge, 2004).
45. Sun, J., Zhang, B. & Katz, H. E. Materials for printable, transparent, and low-voltage transistors. *Adv. Funct. Mater.* **21**, 29–45 (2011).
46. Shaw, J. M. & Seidler, P. F. Organic electronics: introduction. *IBM J. Res. Develop.* **45**, 3–9 (2001).
47. Tahk, D., Lee, H. H. & Khang, D.-Y. Elastic moduli of organic electronic materials by the buckling method. *Macromolecules* **42**, 7079–7083 (2009).
48. Dao, M. & Asaro, R. J. Localized deformation modes and non-Schmid effects in crystalline solids. Part II. deformation patterns. *Mech. Mater.* **23**, 333–334 (1996).
49. Sankaran, S. & O, K. K. Schottky diode with cutoff frequency of 400 GHz fabricated in 0.18 μm CMOS. *Electron. Lett.* **41**, 506–508 (2005).

© 2019 Springer Nature Limited. All rights reserved.

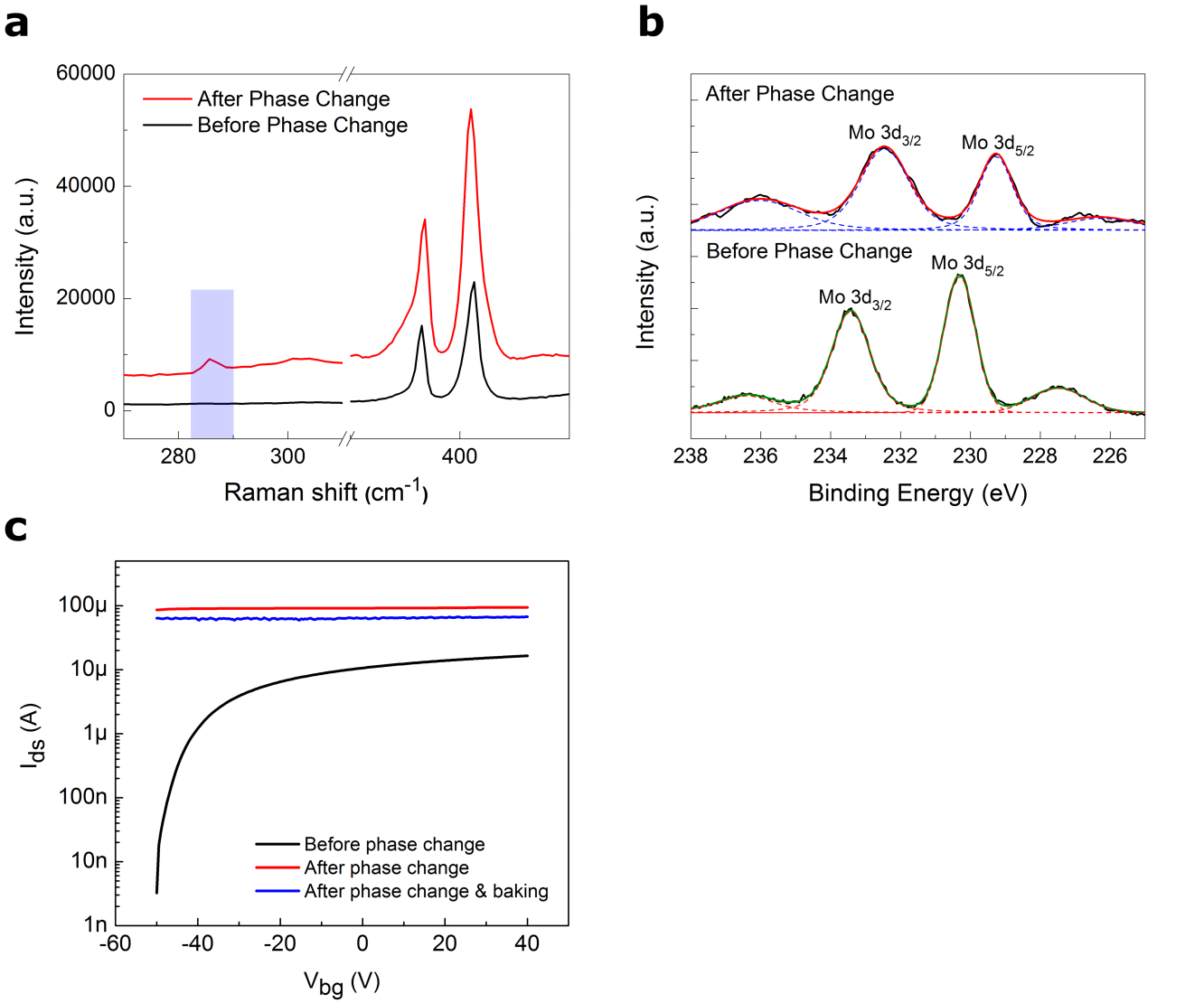

Extended Data Fig. 1 | Spectroscopic and transport study of MoS_2 before and after phase change induced by *n*-butyllithium. a, Raman spectrum of MoS_2 before and after the phase change induced by *n*-butyllithium. A new Raman peak around 286 cm^{-1} was observed after the phase change. **b**, X-ray photoelectron spectroscopy characterization of MoS_2 samples (Mo $3d_{3/2}$ and Mo $3d_{5/2}$ peaks) before and after the 2H-to-1T/1T′ phase change induced by *n*-butyllithium. The Mo $3d_{3/2}$ and Mo $3d_{5/2}$ peaks were red-shifted after the phase change. **c**, *I*–*V* transfer characteristics of a MoS_2 field-effect transistor (FET) on a Si wafer capped with 300 nm SiO_2, before and after phase change. The graph shows the drain current as a function of backgate bias for drain voltage $V_{ds} = 50$ mV, channel length of 830 nm and channel width of 50 μm. The 300-nm-thick SiO_2 serves as the backgate dielectric layer. Black line, pristine MoS_2 FET; red line, MoS_2 FET after phase change through *n*-butyllithium treatment; blue line, post-phase-change MoS_2 FET after baking (180 °C for 3 min). The 1T-phase MoS_2 is unstable in air at room temperature, and part of the 1T region is converted into the 1T′ phase. However, the 1T/1T′ mixture MoS_2 retains metallic *I*–*V* characteristics after baking.

© 2019 Springer Nature Limited. All rights reserved.

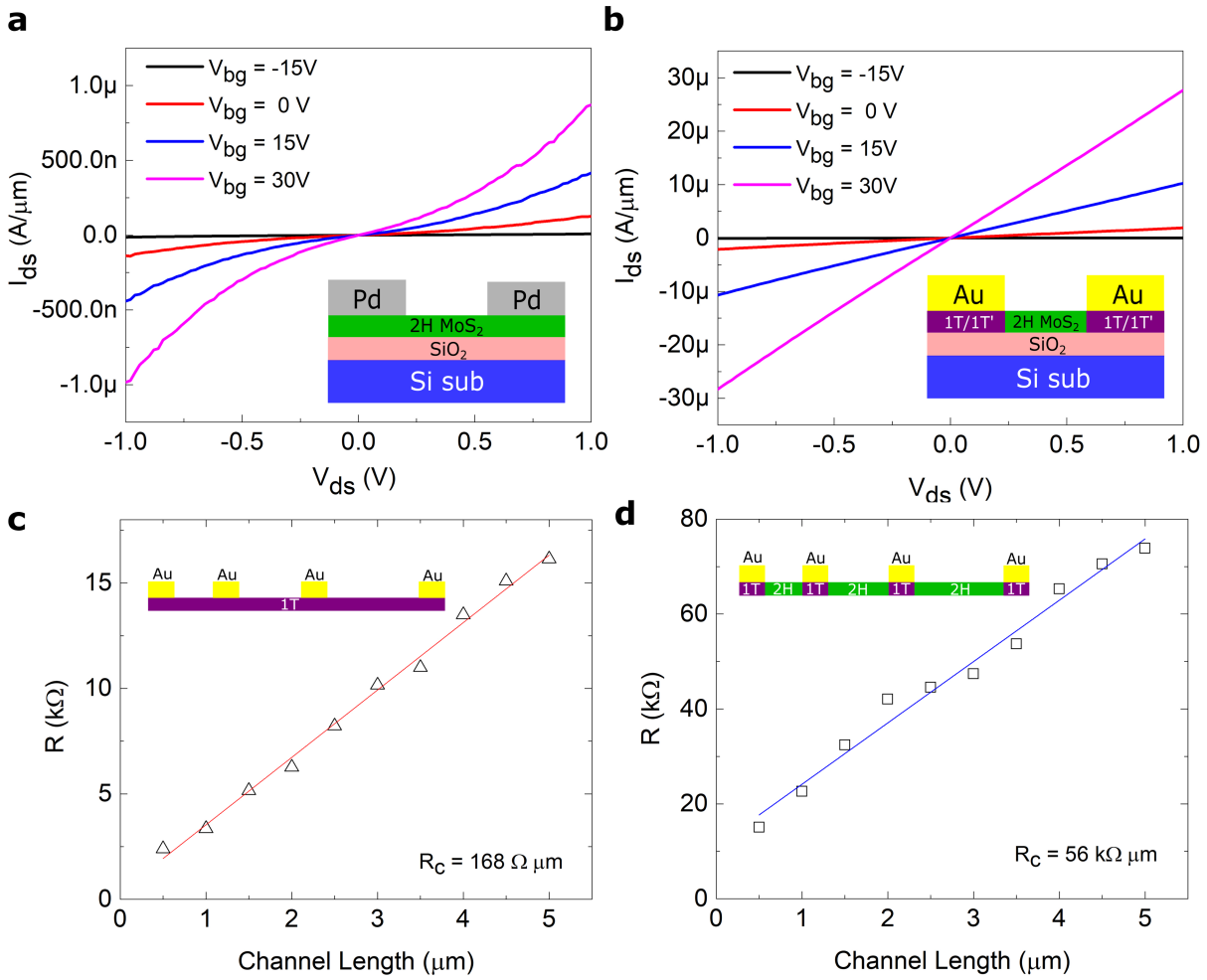

Extended Data Fig. 2 | Investigation of Schottky contact in Pd/2H MoS_2 and Ohmic contact in Au/1T MoS_2/2H MoS_2. a, *I*–*V* characteristics of backgated MoS_2 transistors on Si substrates ('Si sub') capped with 300 nm SiO_2. Channel length, 4 μm. Pd is used as the source/drain contact metal. The nonlinear I_{ds}–V_{ds} characteristics are consistent with the behaviour of a Schottky contact. V_{bg} is the backgate bias. **b**, *I*–*V* characteristics of backgated MoS_2 transistors on Si substrates capped with 300 nm SiO_2. Channel length, 4 μm. The source/drain region of MoS_2 was phase-engineered into the metallic 1T/1T′ phase for use as contact. The linear I_{ds}–V_{ds} characteristics indicate an Ohmic contact. **c**, Transfer-length-method structure of 1T/1T′ MoS_2. The contact resistance between Au and 1T/1T′ MoS_2 is estimated to be about 168 Ω μm. **d**, Transfer-length-method structure of 2H MoS_2 (channel width, 10 μm), in which the contact area is phase-engineered into the 1T/1T′ metallic phase before metal deposition. The contact resistance is estimated to be 56 kΩ μm.

© 2019 Springer Nature Limited. All rights reserved.

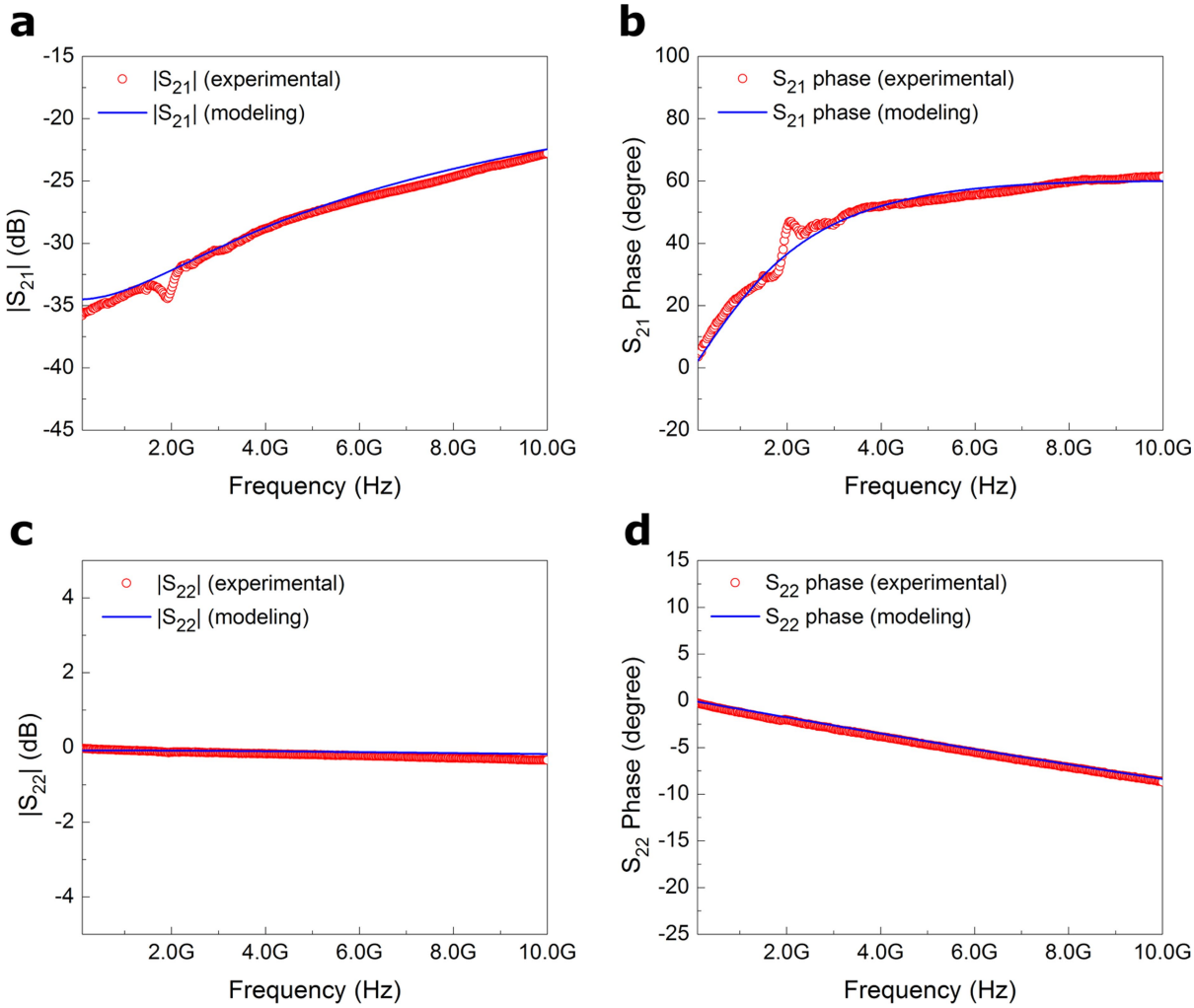

Extended Data Fig. 3 | Comparison of measured S-parameter of the MoS_2 diode and modelled S-parameter based on the equivalent circuit in Fig. 2a. a, Magnitude of S_{21}. **b**, Phase of S_{21}. **c**, Magnitude of S_{22}. **d**, Phase of S_{22}. Red circles, experimental data; blue line, modelled data.

© 2019 Springer Nature Limited. All rights reserved.

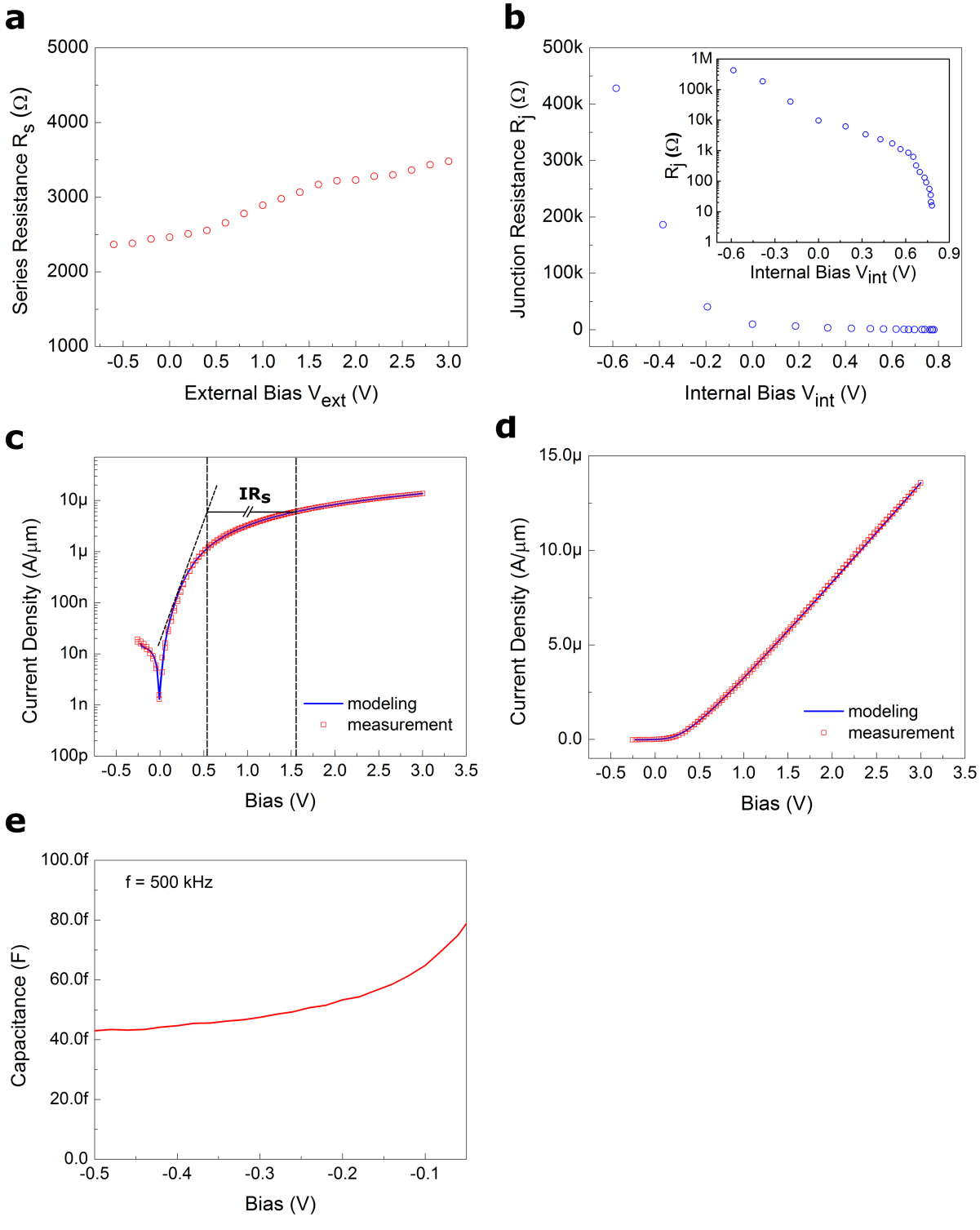

Extended Data Fig. 4 | Resistive and capacitive components of MoS_2 Schottky diode. a, Series resistance, R_s, obtained from S-parameter measurements at different external biases. **b**, Junction resistance, R_j, obtained from S-parameter measurements at different internal voltages. The internal voltage V_{int} is derived from $V_{int} = V_{ext} - I R_s$. **c**, **d**, Quasi-static I–V characteristics of the MoS_2 Schottky diode. The modelling is based on $I = I_s\{\exp[e(V–IR_s)/(nk_BT)]–1\}$, where $I_s = 700$ nA, $n = 2.9$, $R_s = 3{,}500\ \Omega$ and $T = 300$ K. The current density of a MoS_2 phase-junction diode is shown in the logarithmic (**c**) and linear (**d**) scale. Blue line, modelling; red squares, measurements. **e**, C–V characteristics of the MoS_2 Schottky diode at $f = 500$ kHz. When the MoS_2 diode is negatively biased or has a bias around zero, the overall capacitance is about 40–60 fF.

© 2019 Springer Nature Limited. All rights reserved.

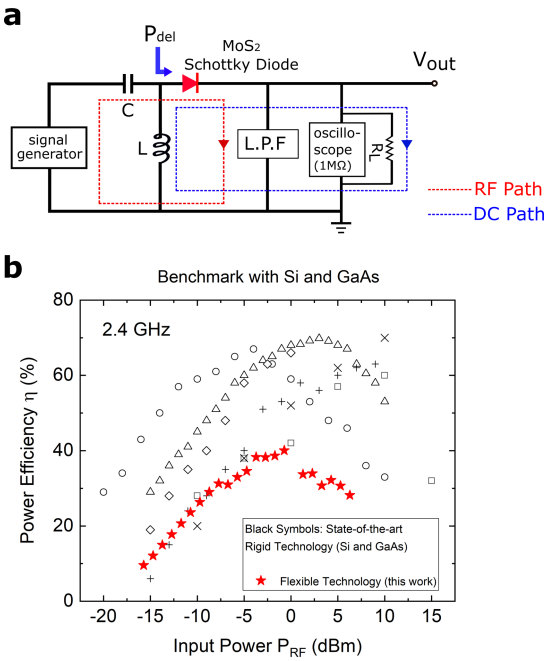

Extended Data Fig. 5 | Demonstration of the MoS_2-based RF energy-harvesting circuit. a, Circuit diagram. The decoupling capacitors at the input can block the d.c. current while permitting flow of RF signals. The d.c. and RF signal paths are indicated by blue and red dashed lines, respectively. The output signal was measured by an oscilloscope with an impedance of 1 MΩ, which was in shunt with a load resistance. The capacitor in this circuit blocks the d.c. current and protects the signal generator, and it is not necessary for the demonstration using the antenna. 'L.P.F.' indicates the low-pass filter and P_{del} is the power delivered to the MoS_2 diode. **b**, Power efficiency of MoS_2-based rectifiers (red stars) compared with state-of-the-art rigid technologies at 2.4 GHz (Si Schottky diodes and GaAs Schottky diodes; black symbols)[35–40]. To ensure a fair comparison, all the data points here show the RF–d.c. conversion efficiency for rectifiers without the antenna effect. In this proof-of-concept demonstration, the flexible MoS_2 rectifiers exhibit competitive power efficiency. We note that the power efficiency was obtained in an academic laboratory before careful optimization. Through optimization of the material engineering, the phase-change process and the matching circuit, the power efficiency of the presented MoS_2-based rectifiers can be further improved.

© 2019 Springer Nature Limited. All rights reserved.

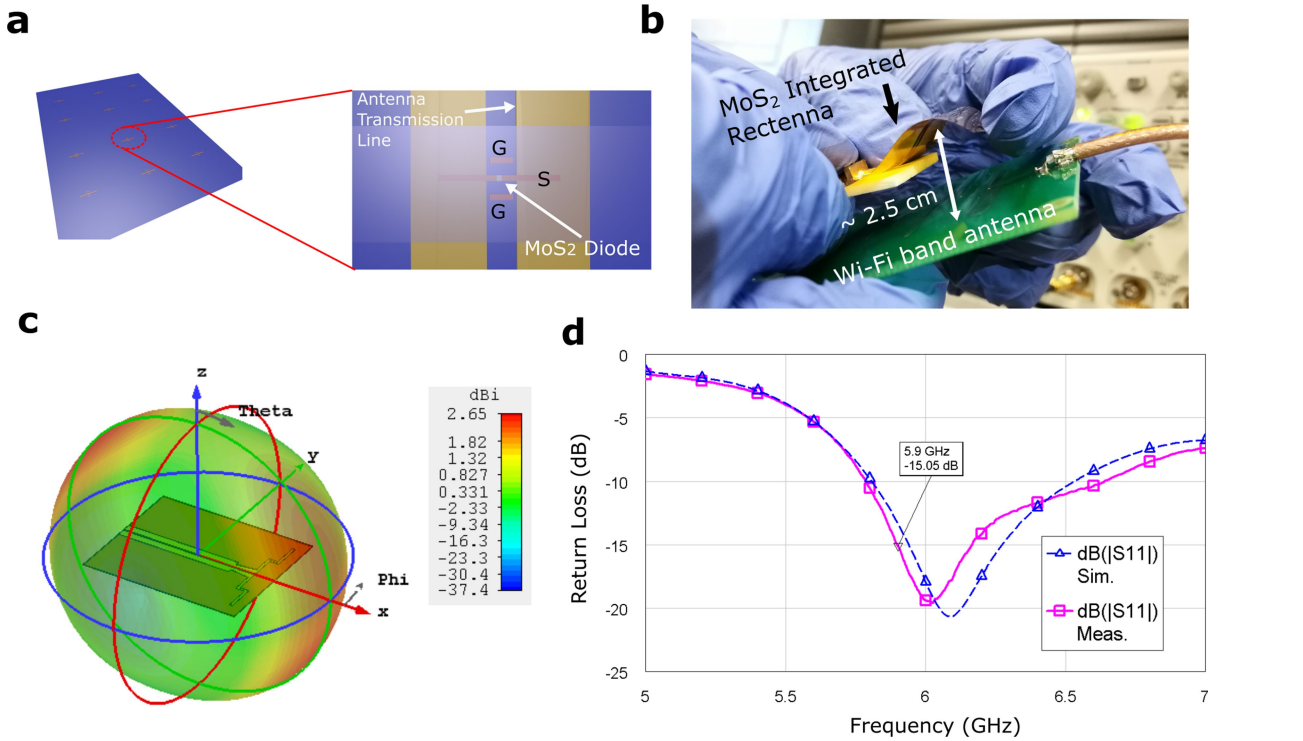

Extended Data Fig. 6 | Fully flexible MoS_2 rectenna harvesting electromagnetic radiation energy in the Wi-Fi band (5.9 GHz). **a**, Fabrication of integrated MoS_2 rectenna. The phase-engineered MoS_2 rectifier arrays are fabricated on Kapton substrates. After high-frequency characterization by S-parameter measurements, we integrated the MoS_2 rectifier with a flexible 5.9-GHz Wi-Fi antenna on the same piece of Kapton film. **b**, Demonstration of energy harvesting of electromagnetic radiation in the 5.9-GHz Wi-Fi band using the as-fabricated flexible MoS_2 rectenna. The input power available to the MoS_2 rectenna was about 3 dBm (about 2 mW). The measurement was carried out in a parallel configuration (as shown in Fig. 3d). The transmitter Wi-Fi-band antenna was powered by a signal generator and approached the receiver antenna of the MoS_2 rectenna. The rectified output voltage V_{out} was about 250 mV, which was measured with an oscilloscope in shunt with a 10-kΩ load resistance. **c**, Simulated directivity pattern of the flexible dipole antenna including the feeding line effect. Theta and phi are the polar and azimuthal angles for spherical coordinates, respectively. The principal y–z, x–z and x–y planes of the antenna are indicated by red, green and blue circles, respectively. The total antenna gain is expected to be only −0.38 dB below the directivity ($D_0 = 2.64$ dB) owing to the low Ohmic loss and the good impedance matching with respect to a reference impedance of 50 Ω. **d**, Return loss of the flexible antenna. The simulation (blue) and measurement (pink) data match well at the operating frequency.

© 2019 Springer Nature Limited. All rights reserved.

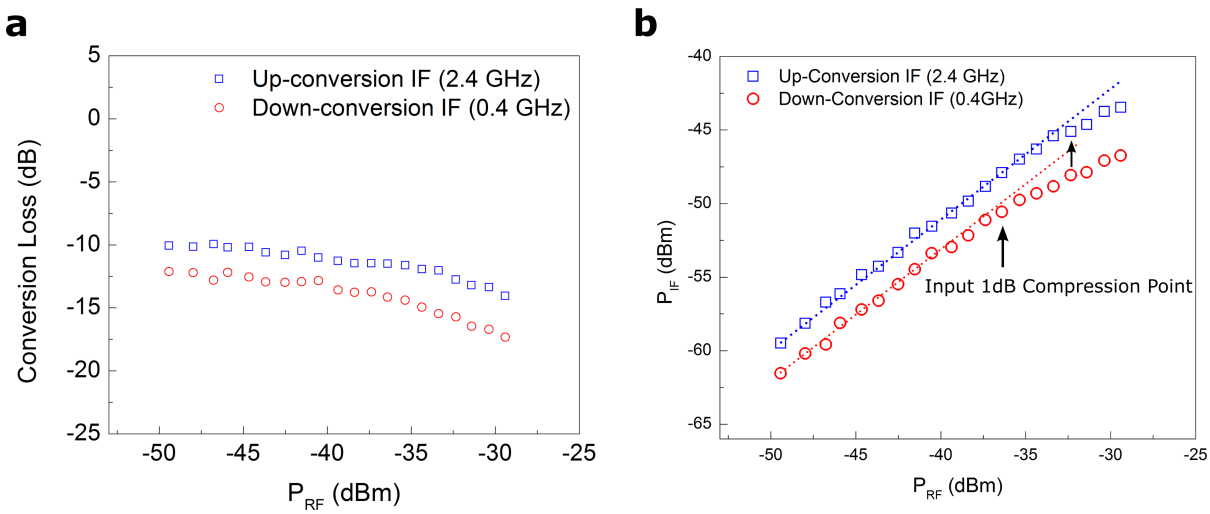

Extended Data Fig. 7 | High-frequency MoS_2 mixers. a, Conversion loss of the MoS_2 mixer at different RF powers delivered at the input. The conversion loss is defined as the power difference between the input RF signal (1.4 GHz) and the output intermediate frequencies (IF; downconverted at 0.4 GHz and upconverted at 2.4 GHz). **b**, Input 1-dB compression point of the MoS_2 mixer. The 1-dB compression point is a measure of an RF mixer's linearity and is defined as the input RF power for which the conversion loss is increased by 1 dB from the ideal. For the upconversion IF of 2.4 GHz, the 1-dB compression point is about −32.3 dBm. For the downconverted IF of 0.4 GHz, the 1-dB compression point is about −36.4 dBm. The high-frequency performance of the flexible MoS_2 mixer can be further optimized by improving the impedance matching, which was not optimized in this proof-of-concept demonstration.

© 2019 Springer Nature Limited. All rights reserved.

Extended Data Table 1 | Comparison of state-of-the-art high-frequency rectifiers

	Materials	Highest f_c (GHz) (defined as -3dB point)	Mobility ($cm^2V^{-1}s^{-1}$)	Maximum Elastic Strain Limit	References
Flexible Technology	MoS_2	10	10-100	23 %	This work, 2, 41
	IGZO	~ 1	1-50	2.9 %	9,10,12,42,43
	Amorphous Silicon	1.6	1-10	5 %	11,44,45
	Organic semiconductor (Pentacene)	0.87	0.001-1	10 %	3,17,46,47
Rigid Technology	Single Crystalline Silicon	400	1400	0.3 %	48, 49

The cutoff frequency f_c, mobility and rigidity parameters of state-of-the-art flexible semiconductors and silicon are listed.

© 2019 Springer Nature Limited. All rights reserved.